COMBINING 3I AND ISCCP CLOUD PARAMETERS FOR BETTER UNDERSTANDING OF CLOUD RADIATIVE EFFECTS

C. J. Stubenrauch[+], W. B. Rossow[#], F. Chéruy[+], N. A. Scott[+], A. Chedin[+]

[+]Laboratoire de Météorologie Dynamique, Ecole Polytechnique, Palaiseau, France

[#]NASA Goddard Space Flight Center, Institute for Space Studies, New York, USA

1. INTRODUCTION

The 3I (Improved Initialization Inversion) algorithm provides temperature and water vapor profiles as well as cloud parameters from HIRS/MSU (High resolution Infrared Radiation Sounder / Microwave Sounding Unit) measurements, available in the framework of the NOAA/NASA Pathfinder Programme. The cloud parameters from this global dataset have been compared to those from the current ISCCP (International Satellite Cloud Climatology Project) dataset as well as from the recently re-processed ISCCP dataset. Due to their relatively good spectral resolution, IR sounders are very useful in the determination of cloud properties (day and night). Their coarse spatial resolution should affect less clouds with a large spatial extension like cirrus clouds. On the other hand, the relatively good spatial resolution of the imagers used in ISCCP is important for the determination of properties of low clouds (day). A first comparison led to a reasonable agreement between 3I cloud parameters and the re-processed ISCCP data. Cirrus cloud identification in the recent ISCCP dataset is improved during day, whereas during night the 3I algorithm alone provides Cirrus information. However, the observation of a systematic effective cloud amount underestimation for low clouds by 3I, especially in the Stratocumulus regions, has led to the development of a new 3I cloud scheme, based on a χ^2 method which is described later on in these proceedings (Stubenrauch et al. 1997b). Comparisons with the re-processed ISCCP agree now much better, especially in the Stratocumulus regions where the cloud type matching improved from about 50% to 75%. Discrepancies in cloud classification appear over partly cloudy regions and when the cloud detection does not agree. Even if the re-processed ISCCP dataset shows a considerable improvement in cloud cover at higher latitudes, there still remain discrepancies with 3I in the polar regions probably due to different cloud-ice identification. Cloud cover in desert zones seems to be overestimated by the re-processed ISCCP in summer. Correlations between cloud optical thickness (ISCCP) and infrared cloud emissivity (3I) agree well with theoretical expectations for high clouds, but mesoscale inhomogeneities in midlevel and low cloud fields cause a different behaviour.

2. DATASETS

2.1 3I cloud parameters

The 3I algorithm suite (Chedin et al. 1985) determines atmospheric temperature and water vapor profiles as well as cloud parameters from HIRS/MSU observations. It is based on 1) the TIGR (Thermodynamic Initial Guess Retrieval) dataset, describing ~1800 atmospheric conditions extracted from ~180000 radiosonde measurements (Escobar 1993) and 2) the fast line-by-line radiative transfer model 4A (Automatized Atmo-

spheric Absorption Atlas) (Scott and Chedin 1981), simulating clear sky radiances and cloudy radiances at 30 pressure levels. Cloud detection is performed at HIRS spatial resolution by 7 (night) / 8 (day) threshold tests, relying very much upon the simultaneous use of HIRS and MSU channels, the latter probing through the clouds. A summary of this cloud detection scheme can be found in Table 2 of (Stubenrauch et al. 1996). Some of the cloud detection tests have been refined: 1) A sea surface temperature (SST) climatology (Shea, Trenberth and Reynolds, 1990) provides the forecast surface temperature for the surface temperature test over ocean. 2) The visible albedo has been corrected for angular effects in the viewing geometry. 3) The maximum brightness temperature test is not performed over land where the relief changes by more than 250m within a 100km x 100km box. 4) At polar latitudes, the SST test threshold is set to 7K instead of 5K. Another important change has been the implementation of seasonal brightness temperature calibration constants by comparing airmass averaged brightness temperatures computed from radiosonde measurements to collocated observed brightness temperatures (Armante et al. 1997).

Cloud parameters are determined from the averaged cloudy pixels within 100km x 100km boxes. One assumes that all cloudy HIRS pixels within a box are covered by a homogeneous single cloud layer. The average cloud-top pressure within a box is obtained by a χ^2 method (Stubenrauch et al. 1997b). Therefore the mean effective cloud amount $N\varepsilon$ over all four channels (4 to 7) in the 15μm CO_2-band (with sounding peaks from 400 to 900hPa) and the 11μm IR window channel, using channel- and cloud level dependent weights, is calculated at 30 cloud pressure levels. Finally one chooses the cloud pressure level which leads to a minimal χ^2.The weights account for the effect of brightness temperature uncertainty inside an airmass on the difference between clear sky and cloudy radiances. Effective cloud amount over a box is calculated by the 3I cloud scheme as the product of the extracted $N\varepsilon$ over cloudy pixels and the fraction of cloudy HIRS pixels within the box.

2.2 ISCCP cloud parameters

The current ISCCP dataset (C-Series of cloud products, Rossow and Schiffer 1991) has been subject to comparisons with various datasets (e. g. Liao et al. 1995, Jin et. al. 1996). Recently, the ISCCP data have been re-processed (D-Series of cloud products, Rossow et al. 1996a).

The most important changes have been the use of the AVHRR (Advanced High Resolution Radiometer) 3.7μm channel for cloud detection at latitudes higher than 50°, a lower IR threshold for cloud detection over land, the recalibration of the visible channel of the AVHRR instrument (Rossow et al. 1996b) and the use of fractal ice particles in the cloud optical thickness calculation (Mishchenko et al. 1996), leading to smaller optical thickness for ice clouds.

ISCCP pixel data (current: CX, re-processed: DX) have a spatial resolution of about 5km and are sampled every 30km. For cloudy pixels, cloud height and optical thickness τ (only during day) are calculated, again assuming a single cloud layer, but this time over a region of 5 km x 5 km. Then follows a classification into one of nine cloud types (only during day), according to three cloud-top pressure intervals and three optical

thickness intervals. In a first step, and always at night, the cloud height is determined by the IR temperature, only. During day, τ is determined from the visible cloud reflectance and a radiative transfer model. If the cloud is not opaque ($\tau_{IR} < 5.5$), the cloud height will be increased in dependence of cloud optical thickness. In such a way, the τ dependent correction accounts for transmission of IR radiation from below the cloud. For the conversion of cloud-top temperature to cloud-top pressure, atmospheric temperature profiles (McMillin and Dean 1982) at a 2.5° spatial resolution from the operational TOVS system (Kidwell 1995) are used. Only one profile per day is provided.

2.3 Combined ISCCP-3I data

The 3I cloud parameters and ISCCP pixel data (AVHRR measurements) from the polar satellite NOAA-10 (observations at ~ 7h30 local time) have been combined into 1° latitude x 1° longitude gridboxes for July 1987 and January 1988. The data have been divided into morning (am) and evening (pm) observations. Starting from the pixel observations allows a simultaneous collocated comparison and combined use of the different cloud information. The ISCCP dataset can be used for the validation of the 3I cloud parameters only during daylight conditions. If during day the 3I cloud parameters seem to be reliable, they should give equally reliable information during night-time, since the 3I method exploits thoroughly the IR domain whereas ISCCP has only 50% of its information available during night.

2.4 ERBE observations

For the analysis of cloud radiative effects, ERBE broadband fluxes (Barkstrom et al.1989) from the ERBE S8 dataset (instantaneous pixel measurements) at a spatial resolution of about 40km at nadir have been averaged into 1° latitude x 1° longitude gridboxes for the same time period. For the spatial collocation one has first to transform the ERBE coordinates, given at the top of the atmosphere, to surface coordinates which are used in the cloud datasets (Stubenrauch 1993). Due to SW intercalibration problems in the original ERBE data, the LW fluxes, obtained as the difference between total and SW fluxes, had to be corrected like in (Thomas et al. 1995), leading to a decrease of 0 to 8 Wm^{-2} for NOAA-10.

3. GLOBAL COMPARISONS

3.1 Cloud type frequencies

In order to get a first impression of the distribution of clouds over the globe, we show a geographical map of the most frequent cloud types in July and in January, obtained from current ISCCP (Figs. 1 a,d), re-processed ISCCP (Figs 1 b,e) and from 3I (Figs 1 c,f).

For clarity, we consider only six different cloud types distinguishing cloud height according to three cloud-top pressure intervals (midlevel clouds between 680hPa and 440hPa) and two 'cloud field opacity' intervals. 3I distinguishes opacity according to effective cloud amount (divided at 90% for high clouds and at 50% for all others). The ISCCP clouds (one cloud type per pixel) within a 1° x 1° grid can be transformed into the six cloud field categories as follows: First, one determines the most frequent cloud height category

within the grid; if the average optical thickness $\tau < 9.4$, the ISCCP clouds belong to the second cloud field category of each cloud height. For midlevel and low clouds, the cloud cover (< 50%) is also used for selecting the second (partly cloudy) cloud field category of the corresponding cloud height.

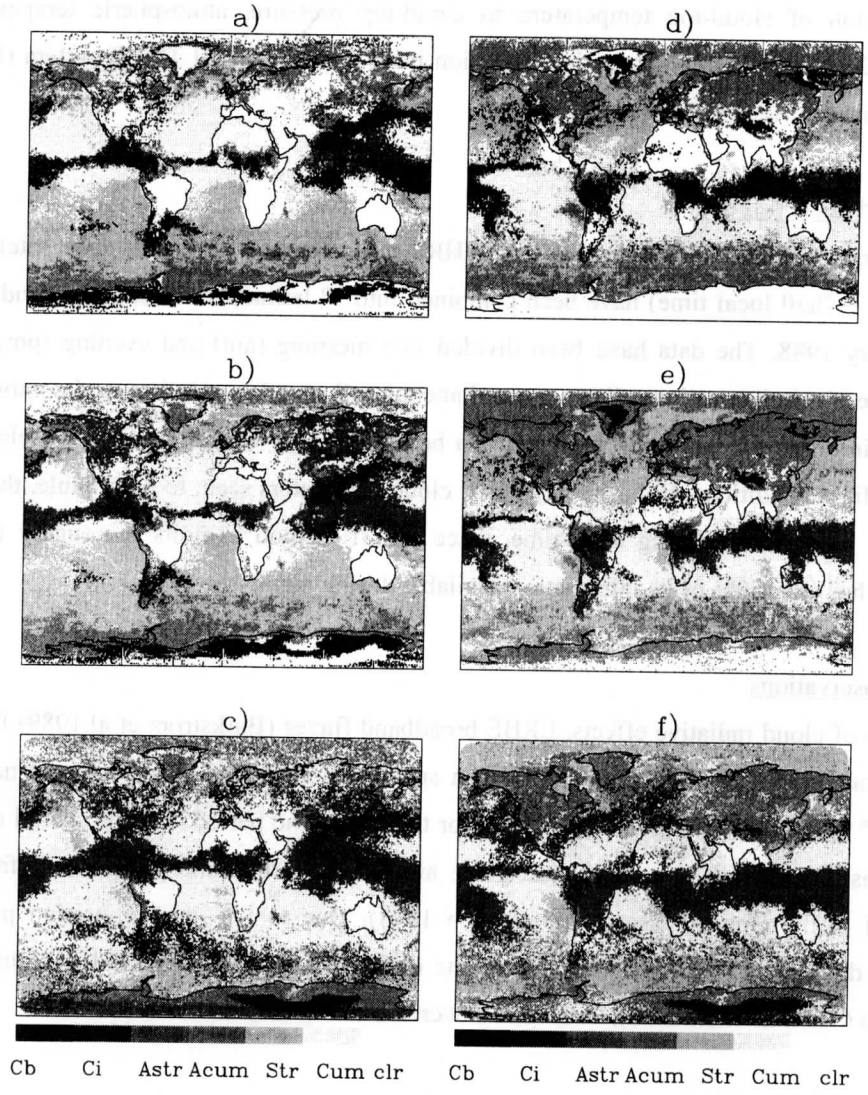

Figs. 1: Geographical maps of the most frequent cloud type at 7h30 am local time in July 1987 (a to c: daylight on Northern hemisphere) and in January 1988 (d to e: daylight on Southern hemisphere) with cloud types identified by a, d) current ISCCP, b, e) re-processed ISCCP and c, f) 3I.

So, each 1° x 1° grid can be covered by (1) Cumulonimbus, (2) Cirrus, (3) Altostratus, (4) Altocumulus, (5) Stratus or (6) Cumulus. The seventh possibility is clear sky.

The re-processed ISCCP dataset (DX) shows an improved identification of cirrus (during day), leading to better agreement with the 3I cloud parameters, as can been seen in Figs. 1. During night, however, 3I cirrus information gives a significant extension of the ISCCP results. Note that at 7h30 am local time there is daylight only in the summer hemisphere. In July there are mostly cirrus over the Northern hemisphere land,

whereas in winter these regions are more covered by midlevel clouds and low clouds. In general, the 3I cirrus zone around the ITCZ (Intertropical Convergence Zone) is still broader than the DX Cirrus zone. With 3I, one can distiguish the Southern Hemisphere storm track zone as well as the North Atlantic storm tracks in winter. During summer, these zones are covered by midlevel and lowlevel clouds. Deserts are covered with more clouds in winter than in summer according to 3I. When there are clouds, they are mostly cirrus in summer, low clouds and Cirrus in winter. ISCCP finds mostly low clouds in summer, but clear sky and Cirrus in winter. The Cumulus clouds in summer could be explained by the ISCCP detection of dust storms in the desertic regions. The Stratus clouds in the Stratocumulus regions appear better in DX than in CX data due to visible calibration corrections leading to an increase of the AVHRR visible radiances on NOAA-10. These Stratus clouds are just as well identified by the new 3I cloud scheme. An interesting feature is the appearance of Cirrus clouds off the Eastern North American coast in July which is confirmed in (Menzel et al. 1997), but not as well identified by ISCCP in the morning hours. A reason for the difference could be that low clouds lie underneath these Cirrus, so that ISCCP would have difficulties to detect them (Jin and Rossow 1997). All the other oceanic regions are mostly covered by partly cloudy lowlevel clouds.

3.2 Cloud radiative effects

The new 3I and re-processed ISCCP cloud properties like effective cloud amount, cloud-top temperature and cloud-top pressure agree globally quite well (Figs 8 in Stubenrauch et al. 1997b). This should also be reflected in the radiative effects of these different cloud types. We study the cloud radiative effects in combination with ERBE fluxes. The cloud-induced longwave (LW) flux change (difference between monthly mean clear sky outgoing LW flux and cloudy outgoing LW flux over a 1° grid) varies between 5 Wm^{-2} (for partly cloudy low-level cloud fields) and 150 Wm^{-2} (for overcast high opaque clouds in the tropics), as can be seen in Figs. 2 for CX, DX and 3I cloud fields over ocean (a-c) and land (d-e) in July. For this analysis, we have brought both cloud type identifications into line by transforming first the ISCCP optical thickness τ and cloud cover into effective cloud amount $N\varepsilon$ (Fig. 4): The IR cloud emissivity ε for each ISCCP pixel is calculated as $\varepsilon = 1 - \exp(-\tau/b)$, where b relates the optical thickness from the VIS to the IR domain; it depends on the cloud phase: $b = 2.13$ for ice clouds and $b = 2.59$ for water clouds (Rossow et al. 1996a). In a second step, one averages the IR cloud emissivities over all cloudy pixels inside a 1° grid. To obtain the ISCCP effective cloud amount, the averaged IR cloud emissivity has yet to be multiplied by the ISCCP cloud cover. We distinguish high opaque clouds (ε>90%), cirrus (90%<ε<50%) and thin cirrus (ε<50%); the mid- and lowlevel cloud fields are separated into mostly cloudy ($N\varepsilon$>50%) and partly cloudy. The zonal mean cloud radiative LW flux changes of DX and 3I clouds are very much alike during day, with an about 10 Wm^{-2} higher warming effect of 3I high opaque clouds. Again, one can distinguish between high opaque and cirrus cloud radiative effects during night only with 3I. Compared to the CX high opaque and cirrus clouds which have radiative effects much closer to each other, there is a considerable improvement in the DX cirrus cloud identification leading to a better radiative distinction, in better agreement with 3I.

These cloud type dependent radiative effects can be compared to global circulation models (Stubenrauch et al. 1997a).

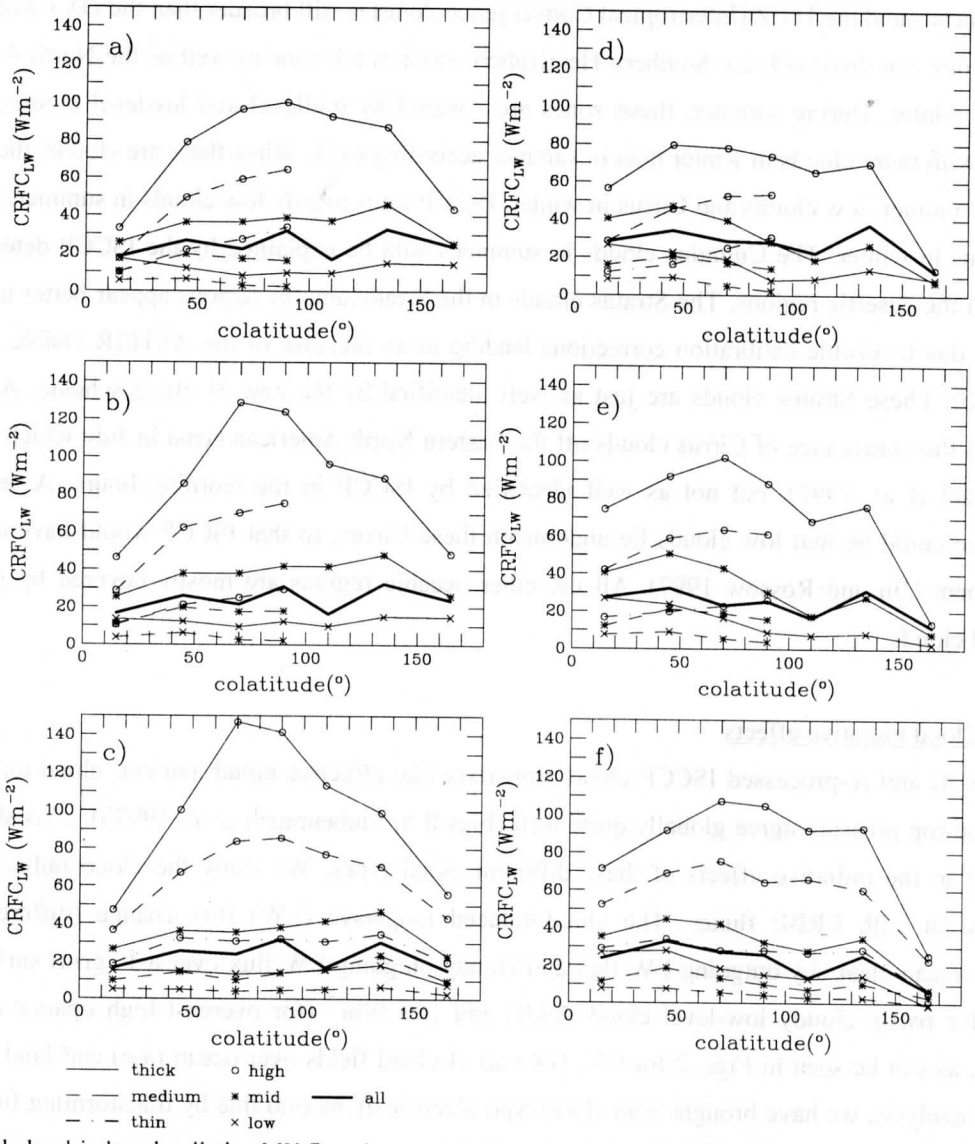

Figs. 2: Zonal cloud-induced radiative LW flux change at 7h30 am local time in July 1987 (daylight on Northern hemisphere) over ocean (a to c) and over land (d to e) with cloud fields identified by a, d) current ISCCP, b, e) re-processed ISCCP and c, f) 3I.

4. REGIONAL COMPARISONS

For a more quantitative comparison, we have selected several geographical regions: 1) Northern midlatitude (40°-70°N) land, NL: containing the North American continent as well as Europe, the southern part of Greenland and the Northern half of Asia, 2) North Atlantic (40°-70°N), NA: the whole ocean between North America and Europe, 3) Southern hemisphere midlatitude (40°-70°S) ocean, SH: the only regions excluded in this band are New Zealand and the Southern part of Southamerica, 4) Stratocumulus regions off the Western coasts, ST: a) STN near California (20°-40°N) in July and b) STS near Namibia (10°-30°S), Australia (10°-40°S) and South America (15°-50°S) in January, and 5) the tropical Warm pool over Indonesia continuing eastwards (10°S-10°N, 70°E-160°W): WP.

In the following, we are interested in four cloud categories: high opaque clouds, cirrus, midlevel and lowlevel clouds. As mentioned above, in the case of ISCCP, the most frequent cloud type within a 1° grid is assigned to the corresponding class. We compare only the re-processed ISCCP with the new 3I cloud scheme. One observes in Figs. 3 a to j very similar frequencies of ISCCP and 3I cloud types during day (in summer). During night (in winter), cirrus clouds are misidentified by ISCCP as midlevel or lowlevel clouds.

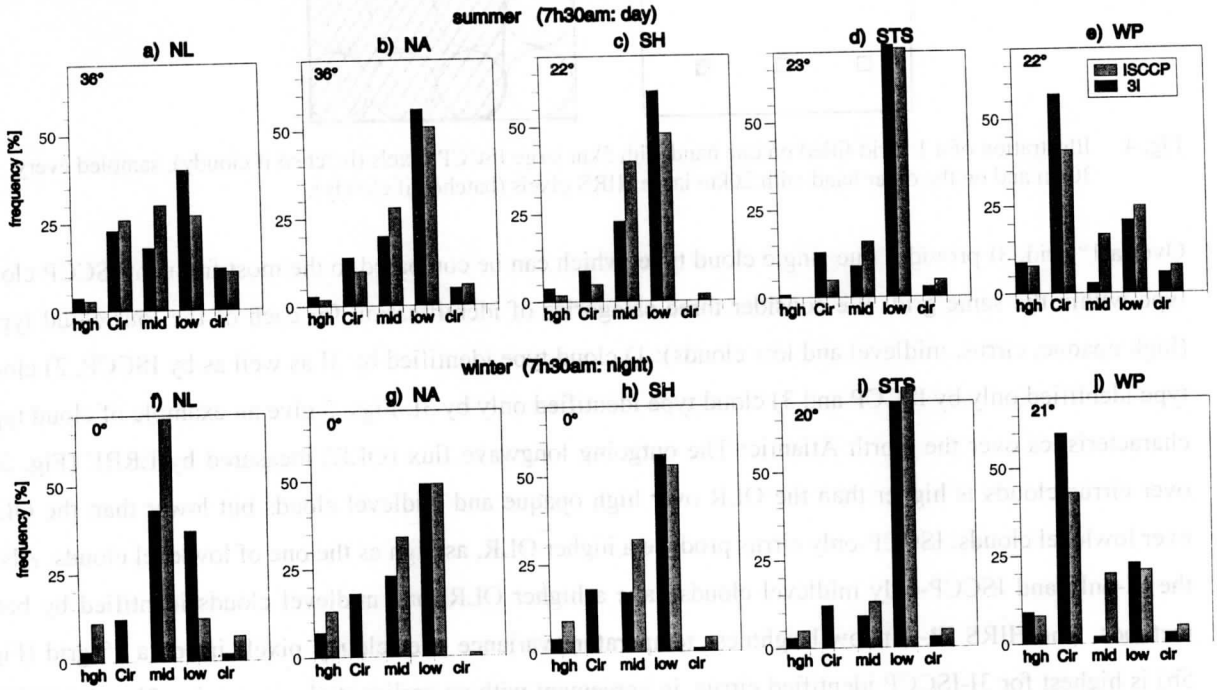

Figs. 3: 3I and re-processed ISCCP cloud type frequencies in summer (a to e: daylight) and winter (f to j: night) over five geographical regions: a, f) Northern hemisphere land, b, g) North Atlantic, c, h) Southern hemisphere ocean, d, i) Southern marine Stratocumulus and e, j) Tropical Warm Pool. For daylight situations, the mean solar zenith angle is indicated.

Whereas each dataset gives very similar regional results, a direct comparison between simultaneous co-located data leads only to a 50 to 75 % simultaneous cloud type matching. Table 1 summarizes the time-space collocated 3I-ISCCP cloud type matching over six regions.

region	NL	NA	SH	STN	STS	WP
3I-DX match	47.4%	64.7%	64.1%	76.4%	72.8%	60.8%

Table 1: Time-space collocated 3I-ISCCP cloud type matching over six geographical geographical regions: Northern hemisphere land, North Atlantic, Southern hemisphere ocean, Northern and Southern marine Stratocumulus and Tropical Warm Pool.

Considering that 3I cloud parameters are calculated once per 1° grid, from the average over all cloudy ~ 20km (at nadir) x 20km large areas within the grid, whereas ISCCP gives information on ~ 5km x 5km large areas sampled out of 30km x 30km large regions, a direct comparison is very difficult (Fig. 4). Disagreement could be explained from inhomogeneities (due to cloud sizes and multilayer clouds) inside

the 1° grids as well as discrepancies in temperature profiles and in cloud cover. This will be tested in the following.

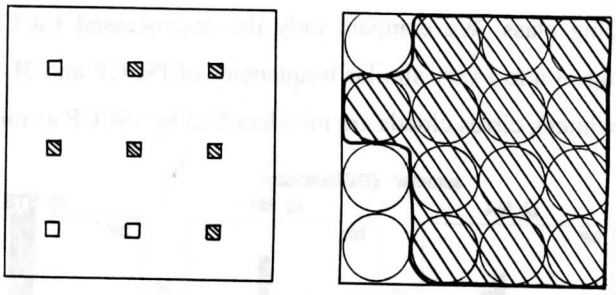

Fig. 4: Illustration of a 1° grid filled on one hand with 5km large ISCCP pixels (hatched if cloudy), sampled every 30km and on the other hand with 20km large HIRS pixels (hatched if cloudy).

Over a 1° grid, 3I provides one single cloud type, which can be compared to the most frequent ISCCP cloud type within the same grid. We consider three categories of identification for each of the four cloud types (high opaque, cirrus, midlevel and low clouds): 1) cloud type identified by 3I as well as by ISCCP, 2) cloud type identified only by ISCCP and 3) cloud type identified only by 3I. Figs. 5 give an example of cloud type characteristics over the North Atlantic: The outgoing longwave flux (OLR) measured by ERBE (Fig. 5a) over cirrus clouds is higher than the OLR over high opaque and midlevel clouds but lower than the OLR over lowlevel clouds. ISCCP-only cirrus produce a higher OLR, as high as the one of lowlevel clouds. Also, the 3I-only and ISCCP-only midlevel clouds have a higher OLR than midlevel clouds identified by both methods. The HIRS IR-window brightness temperature variance over cloudy pixels inside a 1° grid (Fig. 5b) is highest for 3I-ISCCP identified cirrus, in agreement with an earlier study comparing 3I and AVHRR clouds (Stubenrauch et al. 1996). In comparison, the variance is much lower for ISCCP-only cirrus which is as high as for ISCCP only low clouds, leading to the presumption of misidentification of cirrus and partly cloudy mid- and lowlevel cloud fields. This is confirmed in Fig. 5c: the ISCCP cloud cover is lower when 3I and ISCCP do not agree on the cloud type.

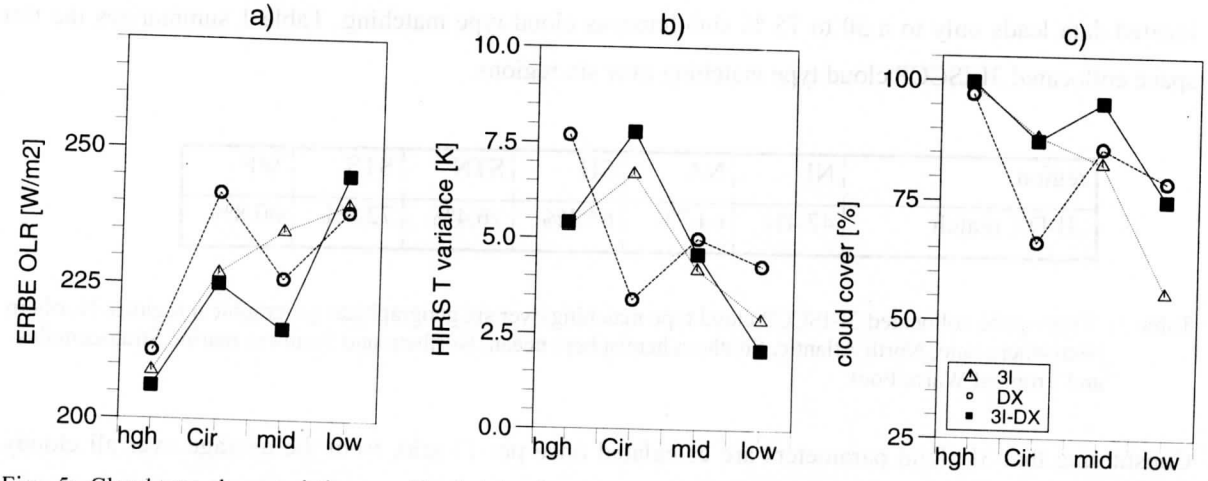

Figs. 5: Cloud type characteristics over North Atlantic at 7h30 local time in July 1987, with three categories of cloud identification: ■ 3I and ISCCP cloud type, ○ ISCCP only cloud type and ▲ 3I only cloud type:
a) ERBE outgoing LW flux (OLR) b) cloudy HIRS IR window brightness temperature variance and
c) ISCCP cloud cover for high opaque, cirrus, mid- and lowlevel clouds.

To study the effect of cloud inhomogeneity on the determination of the effective cloud amount Nε, we consider the ratio of ISCCP effective cloud amount (calculated as in 3.2) and 3I effective cloud amount for high-, mid- and lowlevel clouds as identified by 3I. We distinguish three cases: 1) a homogeneous cloud cover with the same of the nine ISCCP cloud types (see section 2.2) over the whole 1° grid, 2) ISCCP clouds of the same height but with varying optical thickness covering the 1° grid and 3) ISCCP of different height and different optical thickness covering the 1° grid. The Nε ratio is shown for three different regions (NL, NA and SH) in Figs. 6 a to c. We observe that Nε determined by 3I is about the same as the one determined by ISCCP for all cloud heights in the case of a homogeneous grid. Nε determined by 3I is about 30% smaller for all cloud heights in the case of high optical thickness variability. The effect of multilayer clouds leads to a 50% higher Nε for high clouds if one samples the data as in ISCCP, whereas for lowlevel clouds the effect gets compensated.

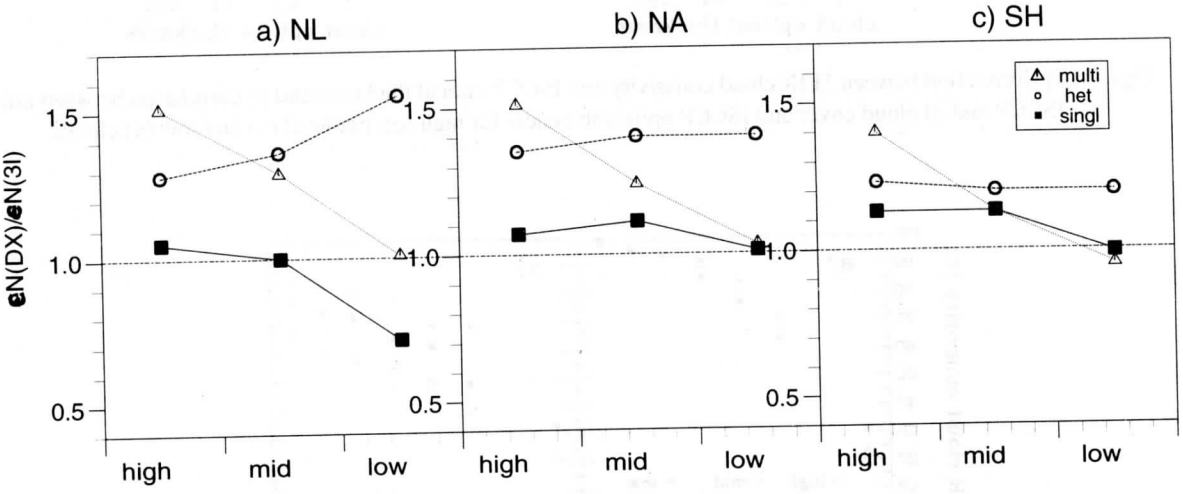

Figs. 6: Ratio of effective cloud amount determined by ISCCP and by 3I for 3I high, midlevel and low clouds over three geographical regions: a) Northern hemisphere land, b) North Atlantic and c) Southern hemisphere ocean. Three situations are shown: ■ homogeneous: same ISCCP cloud type over 1° grid, ❍ same ISCCP cloud height but heterogeneous optical thickness and ▲ multilayer: different ISCCP cloud heights and optical thicknesses.

5. τ-ε CORRELATIONS

In order to match the information of both cloud datasets more quantitatively, we study in Fig. 7a the correlation between cloud optical thickness retrieved by ISCCP and the IR cloud emissivity extracted by 3I (effective cloud amount divided by HIRS cloud cover) over the North Atlantic, separately for high, midlevel and lowlevel cloud fields classified by 3I as well as by ISCCP. The experimental correlation does not agree for low and midlevel clouds with the exponential behaviour for a single layer cloud in the GISS GCM, shown in Fig. 8a. Nevertheless, if one calculates the relationship for the case of several cloud blocks inside a GCM gridbox (Stubenrauch et al. 1997a), one obtains a relationship closer to the observations (Fig. 8b). Again, grid box inhomogeneities play an important role in the relationship between both datasets. This

effect is stronger for low-level clouds due to their smaller sizes: As one can see in Fig. 7b, the ratio of ISCCP and HIRS cloud cover is about one for high clouds at all optical thicknesses, whereas it is smaller for mid- and even still smaller for lowlevel clouds with low optical thickness. Similar effects have been observed in (Sèze and Rossow 1991, Wielicki and Parker 1992).

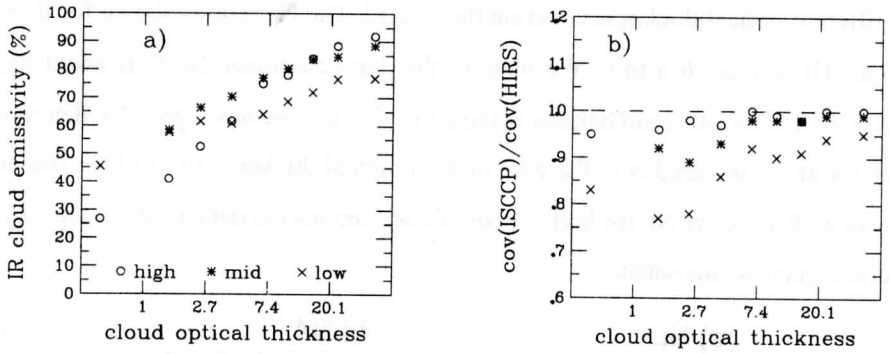

Figs. 7: a) Correlation beween 3I IR cloud emissivity and ISCCP optical thickness and b) correlation between ratio of ISCCP and 3I cloud cover and ISCCP optical thickness for high (o), midlevel (*) and low (x) clouds.

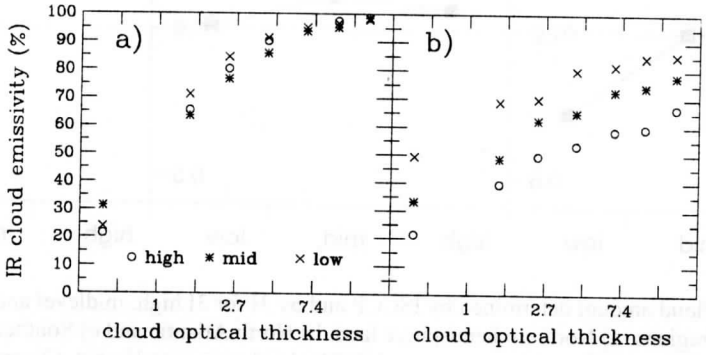

Figs. 8: Correlation beween IR cloud emissivity and optical thickness for high (o), midlevel (*) and low (x) clouds: a) GISS GCM for single layer cloud and b)GISS GCM for multiple cloud blocks

6. CONCLUSIONS

The recently re-processed ISCCP dataset shows an improved cirrus identification during day, in better agreement with the 3I cloud classification. Additional cirrus information during night is provided by the 3I cloud scheme which identifies equally reliable high and low clouds, by using the same χ^2 method. Cloud-induced LW flux change varies between 0 and 150 Wm^{-2}, depending on cloud type and cover as well as on clear sky atmospheric conditions. Again, the improvement of cirrus identification in the re-processed ISCCP dataset leads to a better distinction of cloud radiative effects, in better agreement with 3I. Within most geographical regions, the frequency of the different cloud types identified by ISCCP and 3I is the same. In spite of the different data and methods, the time-space collocated 3I-ISCCP cloud type matching reaches

47% over Northern hemisphere land up to 76% in the Stratocumulus regions. Differences in cloud identification appear over partly cloudy fields and when the cloud detection is not the same. The effective cloud amount as calculated by 3I agrees very well with the one obtained by ISCCP in the case of a uniform cloud type over the 1° grid. Inhomogeneities lead to a smaller 3I effective cloud amount. The correlation between cloud emissivity and optical thickness is very sensitive to inhomogeneities inside the observed area.

7. REFERENCES

Armante R., N. A. Scott, and A. Chedin, 1997: Description of the corrections for radiance biases in the 3I re-analysis of TOVS data, Ninth International TOVS Study Conference Proceedings, Igls, Austria, 20-26 February 1997.

Barkstrom B. R., E. F. Harrison, G. L. Smith, R. Green, J. Kibler, R. Cess, and the ERBE Science Team, 1989: Earth Radiation Budget Experiment (ERBE) archival and April 1985 results. Bull. Amer. Meteor. Soc., 70, 1254-1262.

Chedin A., N. A. Scott, C. Wahiche and P. Moulinier, 1985: The Improved Initialized Inversion method: A high resolution physical method for temperature retrievals from the TIROS-N Series. J. Clim. Appl. Met., 24, 124-143.

Escobar J., 1993: Base de données pour restitution de paramètres atmosphériques a l'échelle globale, Etude sur l'inversion par réseaux de neurones de données des sondeurs verticaux atmosphériques satellitaires présents et à venir. Ph. D. dissertation, Université Pierre et Marie Curie, 167 pp.

Jin Y., W. B. Rossow and D. P. Wylie, 1996: Comparison of the Climatologies of High-Level Clouds from HIRS and ISCCP, J. Clim., 9, no. 11, 2850-2879.

Jin Y., and W. B. Rossow, 1997: Detection of cirrus overlapping low-level clouds, J. Geophys. Res., vol 102, 1727-1737.

Kidwell K. B., 1995: NOAA Polar Orbiter Data Users Guide (TIROS-N, NOAA-6, NOAA-7, NOAA-8, NOAA-9, NOAA-10, NOAA-11, NOAA-12, NOAA-13 and NOAA-14). National Oceanic and Atmospheric Administration, National Environment Satellite, Data and Information Service, Washington DC, 394.

Liao X., W.B. Rossow and D. Rind, 1995: Comparison between SAGE II and ISCCP High-Level Coulds, Part II: Locating Cloud Tops, J. Geophys. Res. 100, 1137-1147.

Mc Millin L. M., and C. Dean 1982: Evaluation of a new operational technique for producing clear radiances, J. Appl. Meteor., vol 21, 1005-1014.

Menzel W. P., D. P. Wylie and K. I. Strabala, 1997: Seven Years of Global Cirrus Cloud Statistics using HIRS, subm. to J. Clim.

Mishchenko M. I., W. B. Rossow, Macke A. and Lacis A. A., 1996: Sensitivity of cirrus cloud albedo, bidirectional reflectance and optical thickness retrieval accuracy to ice particle shape, J. Geophys. Res. 101, no D12, 16973-16985.

Rossow W. B., A. W. Walker, D. Beuschel and M. Roiter, 1996a: International Satellite Cloud Climatology Project (ISCCP): Description of New Cloud Datasets. WMO/TD-No.737, World Climate Research Programme (icsu and WMO), Geneva, February 1996, 115pp.

Rossow W. B., C. L. Brest and M. Roiter, 1996b: International Satellite Cloud Climatology Project (ISCCP) Radiance Calibration Report-Update. WMO/TD-No.736, World Climate Research Programme (ICSU and WMO), Geneva, 71pp.

Rossow W. B. and R. A. Schiffer, 1991: ISCCP Cloud Data Products. Bull. Amer. Meteor. Soc., 72, 1-20.

Scott N. A., and A. Chedin, 1981: A fast line-by-line method for atmospheric absorption computations: The Automized Atmospheric Absorption Atlas, J. Appl. Meteor., 20, 802-812.

Sèze G., and W. B. Rossow, 1991: Effects of satellite data resolution on measuring the space/time variations of surfaces and clouds, Int. J. Rem. Sens., vol 12, 921-952.

Shea D. J., K. E. Trenberth and R. W. Reynolds, 1990: A global monthly Sea Surface Temperature Climatology, NCAR technical note, TN-345+STR, 167pp.

Stubenrauch C. J., 1993: Co-location of AVHRR, ERBE and HIRS/MSU data. Laboratoire de Météorologie Dynamique Internal Note No. 185, 9 pp.

Stubenrauch C. J., N. A. Scott and A. Chedin, 1996: Cloud Field Identification for Earth Radiation Budget Studies: I) Cloud Field Classification using HIRS/MSU Sounder Measurements, J. Appl. Met., Vol 35, 416-427.

Stubenrauch C. J., A. D. Del Genio and W. B. Rossow, 1997a: Implementation of Sub-Grid Cloud Vertical Structure inside a GCM and its Effect on the Radiation Budget, J. Clim., vol 10, no 2, 273-287.

Stubenrauch C. J., A. Chedin, R. Armante and N. A. Scott, 1997b: A new Approach for Cloud Parameter Determination in the 3I Algorithms, Ninth International TOVS Study Conference Proceedings, Igls, Austria, 20-26 February 1997, 11 pp.

Thomas D., J. Ph. Duvel and R. S. Kandel, 1995: Diurnal Bias in Calibration of Broad-Band Radiance Measurements from Space, IEEE Transactions on Geosc. and Rem. Sens., vol 33, no 3, 670-683.

Wielicki B. A., and L. Parker, 1992: On the determination of cloud cover from satellite sensors: The effect of sensor spatial resolution, J. Geophys. Res., vol 97, 12799-12823.

TECHNICAL PROCEEDINGS OF

THE NINTH INTERNATIONAL TOVS STUDY CONFERENCE

Igls, Austria

20-26 February 1997

Edited by

J R Eyre

Meteorological Office, Bracknell, U.K.

Published by

European Centre for Medium-range Weather Forecasts
Shinfield Park, Reading, RG2 9AX, U.K.

May 1997